Fatty acids are not a significant contributor to the TCA cycle in cancer cell lines: evidence of incomplete fatty acid oxidation.

Nancy T Santiappillai[1], Mariam F Hakeem-Sanni[1], Masih Ghasemi[1], Anabel Withy[1], Lake-Ee Quek[2], Andrew J Hoy[1,*]

[1] School of Medical Sciences, Charles Perkins Centre, The University of Sydney, Sydney, New South Wales, 2006, Australia.

[2] School of Mathematics and Statistics, Charles Perkins Centre, The University of Sydney, Sydney, New South Wales, 2006, Australia.

[*] Contact. Tel: +61 2 9351 2514; Email: andrew.hoy@sydney.edu.au

ABSTRACT

Fatty acid (FA) oxidation (FAO) is upregulated in many cancers, which has been contextualised to thereby be significantly fuel the TCA cycle and generate vast amounts of ATP to support cancer cell viability. However, direct evidence of this is lacking. Here, we set out to determine the capacity of FAO in a pan-cancer setting and if this relates to the amount of carbon FAO contributes to the TCA cycle relative to other substrates. We profiled the baseline FAO rate and capacity of 27 cancer cell lines from 10 tissue origins, and then selected 6 cancer cell lines that represented the diversity of this panel. Despite the diverse range of FAO rates, we consistently found that exogenous long-chain FAs (LCFAs) were a minor (<10%) TCA cycle substrate in all cells compared to glucose and glutamine. Glucose withdrawal significantly increased FAO rates, while glucose and/or glutamine deprivation marginally increased incorporation of ^{13}C-palmitate into TCA cycle metabolites. Palmitate alone modestly assisted cataplerosis but did not sustain TCA cycle fluxes, leading to reduced cell viability. The low contribution of fatty acids to the TCA cycle in cancer cells may be explained by incomplete oxidation of LCFAs of varying chain lengths of saturations to produce shortened acyl-carnitines. Overall, our results provide significant insights into mitochondrial FA metabolism in cultured cancer cells and challenges the belief that the oxidation of FAs is a complete process, contributing significant fuel for the TCA cycle and ATP generation.

Keywords

Mitochondria, cancer, fatty acid oxidation, parallel stable isotope tracing, metabolomics

30 # Introduction

31 Many cancers, including glioma[1], prostate[2] and lung cancers[3], exhibit increased expression of
32 genes involved in fatty acid oxidation (FAO), and been reported to be associated with poor
33 prognosis. Drugs targeting FAO reactions are effective against particular cancers and have been
34 reported to reduce ATP production in pancreatic ductal adenocarcinoma[4], and sensitise
35 leukemia cells to proapoptotic effects by increasing membrane permeability[5]. Of these, the
36 inhibition of carnitine palmitoyltransferase 1 (CPT1)[6,7], the rate limiting enzyme in FAO[8],
37 directly impacts ATP production and leads to reduced cell viability in various cancers including
38 glioblastoma[9], prostate cancer[10], myeloma[11] and glioma[12]. Others have shown that CPT1
39 inhibition leads to altered mitochondria structure or morphology before impacting
40 respiration[13,14]. A major limitation to these studies is that, in general, they assess FAO in the
41 absence of measures of other mitochondrial fuels. As such, they fail to consider metabolic
42 plasticity and flexibility that likely supports cancer cell viability and disease progression.

43 FAO is consistently framed through the lens of cellular respiration, as it produces NADH,
44 $FADH_2$ and acetyl-CoA that are substrates for ATP production [15,16]. Inherent to this framework
45 is the assumptions that arise from textbook biochemistry, whereby one molecule of palmitate
46 generates eight acetyl-CoA units and 129-132 ATP, compared to only 36 ATP from one
47 molecule of glucose. As such, any increase in FAO much equate to increased ATP production,
48 irrespective of whether FAO is a major carbon source to the TCA cycle or not. Glucose and
49 glutamine are significant sources of carbons to the TCA[17,18], yet are rarely assessed alongside
50 FAs. We recently reported that exogenous long chain FAs (LCFAs) are minor carbon sources
51 for the TCA cycle compared to glucose and glutamine in prostate cancers (PCa)[19], despite PCa
52 known to possess high FAO rates[20]. In this study, we set out to examine the dynamic flexibility
53 of FAO rates differ between cancer types and how these correlate to TCA cycle fluxes.

54 # Results

55 ## Fatty acid oxidation in cancer cells showed diverse rates and spare capacity.

56 We measured FAO rates using [1-^{14}C]-palmitate derived CO_2 production in 27 cancer cells
57 from 10 different origin sites (Figure 1A) with the aim of identifying a spectrum of phenotypes.
58 We saw striking differences in baseline FAO rates within and between cancer types (Figure
59 1B). Notably, PCa cells, in general, had the highest FAO rates compared to other cancer types
60 (Figure 1B).

61 We also sought to gain insights into the plasticity of FAO. As FAO increases in response to
62 inhibition of glycolysis or low glucose uptake, including in glioblastoma and breast cancer
63 cells[21,22], we quantified FAO rates in glucose-free conditions. As predicted, FAO was increased
64 in all cell lines in glucose-free media, but the magnitude of increase was variable (1- to 8- fold).
65 Interestingly, the magnitude of change in FAO from 5 mM glucose to glucose-free did not
66 correlate with baseline values (Figure 1C and S1A). We further examined the relationship
67 between FAO rates and media glucose levels and determined that FAO increased only when
68 media glucose was 1 mM or below (Figure S1B and S1C). Conversely, we showed that FAO
69 was not dependent on nutrient gradients since a 5-fold increase in media palmitate did not
70 increase FAO rate in the presence of 5 mM glucose (Figure S1D).

71 Based on the fold change (FC) in FAO rates +/- 5 mM glucose as a measure of plasticity, we
72 selected 6 cell lines that ranged from high (above 4-fold), mid (2-4-fold) and low (0-2-fold).
73 These cells were ranked in terms of increasing fold changes of FAO rate (-glucose to
74 +glucose): MDA-MB-231 and MCF-7 (breast), MIA PaCa-2 (pancreatic), DO4 (melanoma),
75 HEPG2 (liver), and HT-29 (colorectal) (Figure 1D and S1A). Among these cell lines, CPT1a
76 protein levels spanned 0.1-to-2.3-fold compared to MDA-MB-231 cells (Figure 1E), yet there
77 was no correlation between CPT1a protein levels baseline (+ glucose; R^2=0.07, p=0.26) or

maximal FAO (-glucose; R^2=0.01, p=0.64) rates. Interestingly, there was a negative correlation between the protein levels of CPT1a and FAO FC (R^2=0.34, p=0.01) (Figure 1F). This suggested that cells with low CPT1a protein levels had greater FAO flexibility, whereas cells with high CPT1a protein levels were already functioning close to their maximal FAO capacity. We also questioned where the range of FAO rates were simply explained by the cellular levels of active mitochondria. However, there was relationship between active mitochondria and basal, maximal, or FC FAO (Figure S1E). Collectively, these results show that glucose availability had the greatest influence on FAO rates, followed by factors intrinsic to the cell lines rather than tissue types.

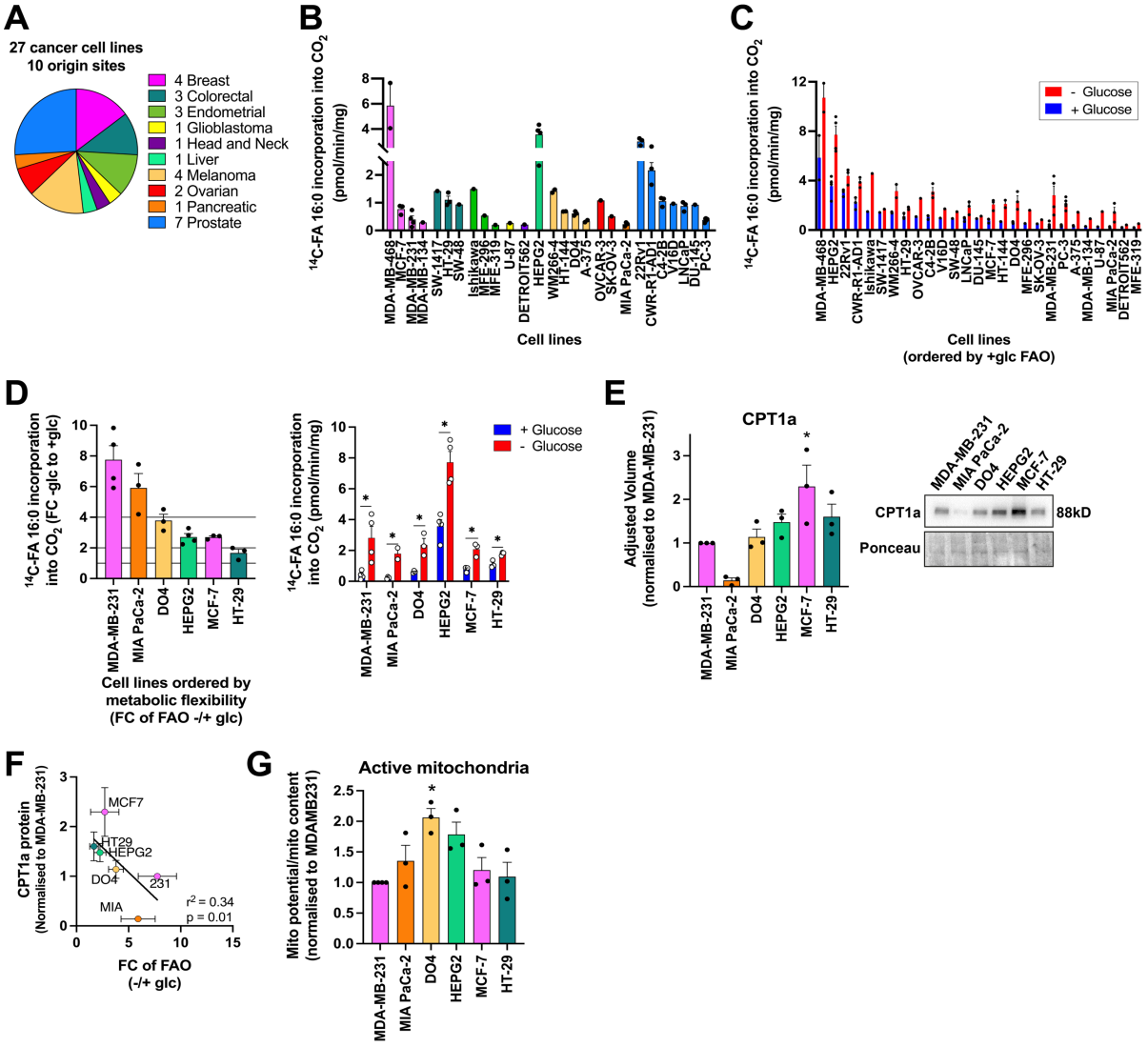

Figure 1. FAO in a panel of heterogeneous cancer cells from different tissue origin sites.

(A) Panel of 27 cancer cell lines from 10 tissue origin sites measured for FAO capacity.
(B) Basal [1-^{14}C]-FA 16:0 oxidation rates in the presence of glucose. Cells ordered by cancer origin site. N=1-5 per cell line.
(C) [1-^{14}C]-FA 16:0 oxidation rates in the presence (blue) or absence of glucose (red). N=1-5 per cell line.
(D) Selection of 6 cell lines based on a range of fold change (FC) differences (<2 to >7, left) of FAO -/+ glucose (right). N=3-4 per cell line.
(E) Quantification of CPT1a protein levels normalised to MDA-MB-231 cells. One of three immunoblot experiments is shown.
(F) Correlation between CPT1a protein levels and the fold changes of FAO -/+ glucose. Error bars represent ± SD. P and r^2 values by linear regression.
(G) Active mitochondria as a fraction of mitochondrial potential to mitochondrial content normalised to MDA-MB-231 cells. N=3-4 per cell line.

Graphs show mean ± SEM unless stated otherwise. *p<0.05 by One-way ANOVA with Dunnett's multiple comparisons test, unless stated otherwise. See also Figure S1.

Palmitate is a minor TCA cycle carbon source compared to glucose and glutamine.

FAO is commonly assumed to be a major contributing source to the TCA cycle via the production of acetyl-CoA to support ATP production[15,16]. Taking advantage of our panel of cancer cell lines diverse FAO activity (Figure 1), we sought to determine whether these FAO rates corresponded to FA-derived carbons arriving at the TCA cycle, in comparison to the major TCA cycle substrates glucose and glutamine. We used a parallel tracing strategy that consisted of feeding cells uniformly labelled ^{13}C-glucose, glutamine, or palmitate (FA 16:0) and quantifying the enrichment of TCA cycle intermediates in our panel of 6 cancer cell lines (Figure 2A). We first identified that 6 hours was the optimal tracing duration as media substrate levels were not fully depleted nor was there evidence of impaired substrate uptake (Figure S2A). This was critical as we showed that removal or very low levels of extracellular glucose has a striking effect on FAO rates (Figure 1). As such, the depletion of glucose from the media after 12 and 24 hours likely impacts ^{13}C-palmitate metabolism. This rapid rate of media glucose consumption can somewhat be avoided by doubling the media volume (Figure S2B).

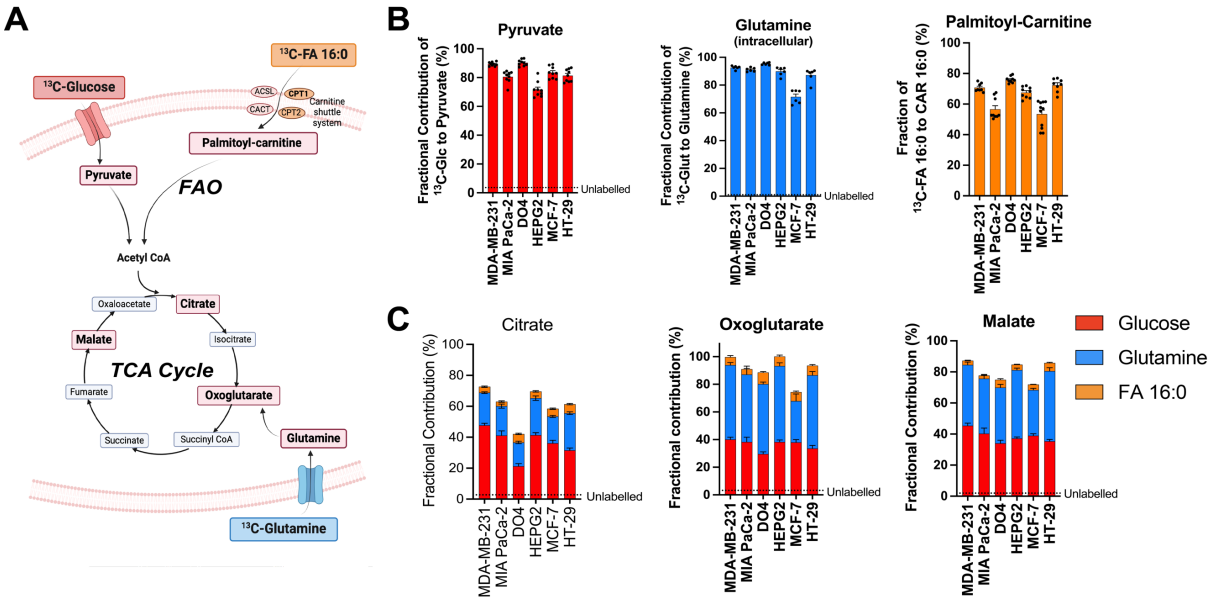

Figure 2. Palmitate is a minor contributing substrate source to the TCA cycle compared to glucose and glutamine.

(A) Schematic of [U-^{13}C]-glucose (5 mM), glutamine (1 mM), or FA 16:0 (150 µM) tracing into the TCA cycle and precursor metabolites for 6 hours.
(B) Fractional contribution of [U-^{13}C]-glucose to pyruvate (red), [U-^{13}C]-glutamine to intracellular glutamine (blue), [U-^{13}C]-FA 16:0 to palmitoyl-carnitine (orange) after 6 hours of labelling. N=9 per cell line. Level of natural enrichment of metabolite standards indicated.
(C) Fractional contributions of [U-^{13}C]-glucose, glutamine, or FA 16:0 to citrate, oxoglutarate and malate. N=9 per cell line.

Graphs show mean ± SEM unless stated otherwise. See also Figure S2.

Next, we quantified the relative contributions of exogenous palmitate, glucose, and glutamine to TCA cycle metabolites. We observed significant enrichments of key precursor pools; >80% enrichment of pyruvate from ^{13}C-glucose, >60% enrichment of intracellular glutamine from extracellular ^{13}C-glutamine, and >56% enrichment of palmitoyl-carnitine from ^{13}C-palmitate (Figure 2B). Despite being taken up and activated by cells, palmitate minimally contributed (<6%) to TCA cycle metabolites citrate, oxoglutarate and malate, compared to glucose (30-50%) and glutamine (20-45%) (Figure 2C). Strikingly, this pattern was observed in all cell lines, and there were no major distinctive patterns in cells with high (MDA-MB-231, MIA PaCa-2) or low (MCF-7, HT-29) FAO activity (Figure 1D). Therefore, these results show that exogenous palmitate is a minor contributing substrate to the TCA cycle in the presence of physiological glucose and glutamine, irrespective of cellular FAO activity as measured by $^{14}CO_2$ production (Figure 1).

141 **Exogenous palmitate is insufficient to maintain TCA cycle activity in the**
142 **absence of glucose and glutamine.**

143 Several studies have shown that inhibiting FAO in glucose-deprived conditions or co-targeting
144 with glycolysis inhibitors decreases respiration, cancer cell viability and tumour volume[21,23].
145 Since we observed that FAO rates increase in glucose-deprived conditions (Figure 1C and 1D),
146 we reasoned that FAO becomes the primary carbon source for the TCA cycle in this setting.
147 Firstly, we observed increased ^{13}C-palmitate enrichment into citrate in glucose-free, and
148 glucose-/glutamine-free conditions in all cells except for the DO4 cells (Figure 3A and 3B).
149 However, the contribution of palmitate to citrate broadly remained <13%. This increased
150 fuelling of the TCA cycle by FAO in glucose-/glutamine-free conditions was also associated
151 with other changes in metabolism. Specifically, we observed increased m+2 and, to a greater
152 extent, m+4 labelling of citrate that correspond to the 1st and 2nd turns of the TCA cycle,
153 respectively (Figure 3C). These results suggest that palmitate-derived carbons go through
154 multiple rounds of the TCA cycle when glucose, or both glucose and glutamine are absent in
155 culture media.

156 Another striking shift in palmitate metabolism in glucose-/ glutamine-free media conditions
157 was the enrichment of the cataplerosis metabolites glutamate and aspartate (Figure 3A). Under
158 glucose and glutamine replete conditions, the conversion of palmitate carbon into glutamate
159 and aspartate was minimal (~2-6%) (Figure 3D). However, a shift in palmitate carbon
160 utilisation was observed in glucose and glutamine-deprived medium (~10-19%) and to a lesser
161 extent in glucose-deprived medium (~5-14%) (Figure 3D). Overall, these results indicate that
162 cancer cells have the capacity to increase the catabolic conversion of palmitate into TCA cycle
163 metabolites and amino acids, but this only occurs in extreme conditions when extracellular
164 glucose and/or glutamine are unavailable.

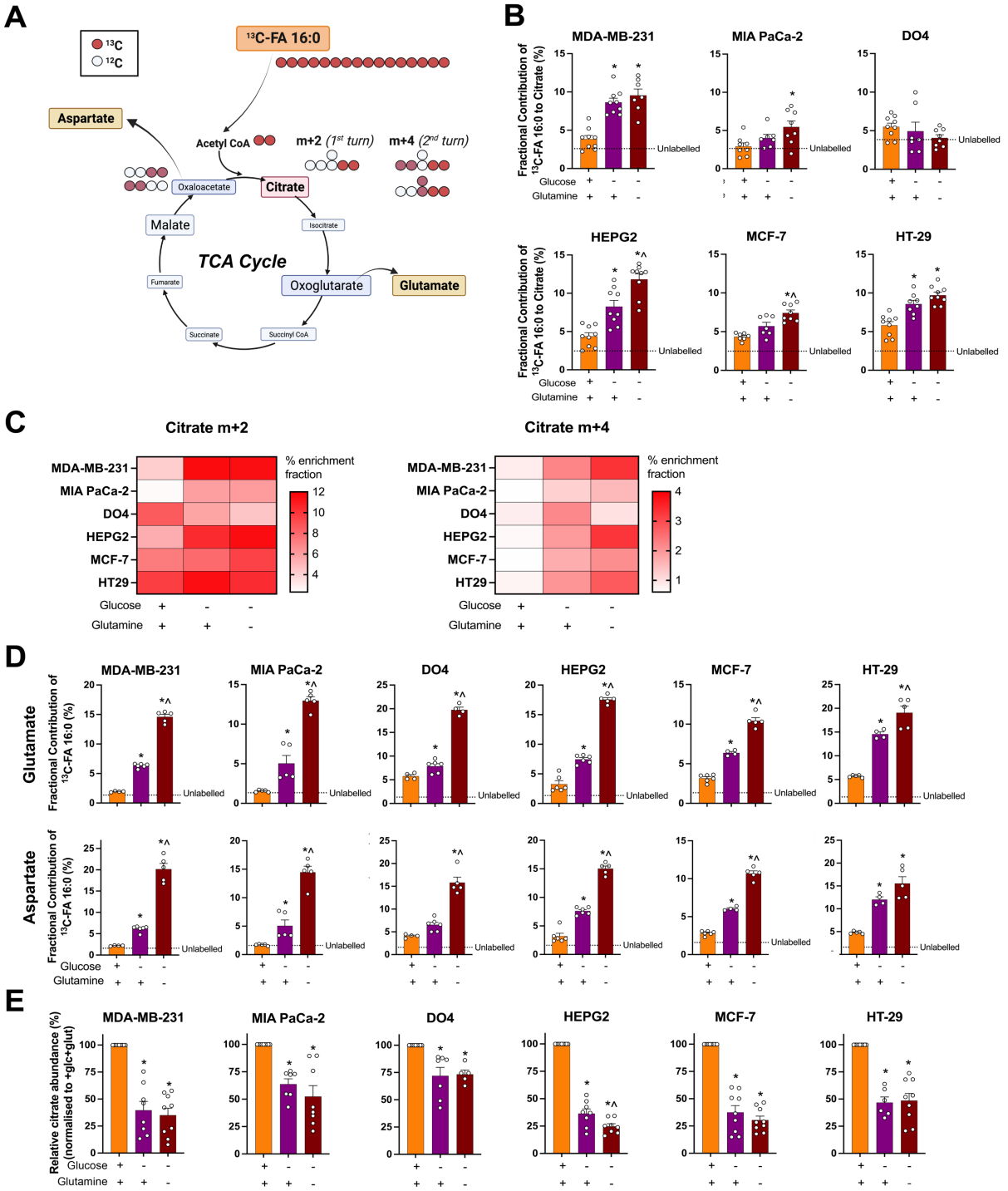

Figure 3. Palmitate alone cannot maintain TCA cycle activity.

(A) Schematic tracing conversion of [U-^{13}C]-FA 16:0 to citrate m+2 and m+4, glutamate, aspartate.
(B) Fractional contribution of [U-^{13}C]-FA 16:0 to citrate +glucose/+glutamine, -glucose/+glutamine, or -glucose/-glutamine. N=9 per cell line.
(C) Enrichment fraction (%) of [U-^{13}C]-FA 16:0 to m+2 and m+4 citrate + glucose/+glutamine, -glucose/+glutamine, and -glucose/-glutamine. N=9 per cell line.
(D) Fractional contribution of [U-^{13}C]-FA 16:0 to glutamate and aspartate +glucose/+glutamine, -glucose/+glutamine, or -glucose/-glutamine. N=4-6 per cell line.
(E) Relative abundance (normalised to +glucose/+glutamine) of [U-^{13}C]-FA 16:0 to citrate. N=6-9 per cell line.

175 Graphs show mean ± SEM. P<0.05 by One-way ANOVA with Dunnett's multiple comparisons test, *compared
176 to +glucose/+glutamine, ^compared to -glucose/+glutamine. See also Figure S3.

177 We observed increased incorporations of palmitate-derived carbons into TCA cycle metabolites
178 in glucose-/ glutamine-free settings, and next questioned whether this was sufficient to
179 maintain TCA cycle activity. By contrast to the enrichment results, the relative abundance of
180 citrate, oxoglutarate, and malate was significantly reduced in glucose-/ glutamine-deprived
181 conditions compared to nutrient-replete conditions (Figure 3E and S3B). These changes
182 preceded the decreased cell viability that occurs between 6 to 24 hours (Figure S3A). Taken
183 together, these findings demonstrate that palmitate remained insufficient to sustain TCA cycle
184 metabolite levels and activity and cell viability despite the dynamic changes in FA metabolism
185 of cancer cells cultured in glucose-/glutamine-free conditions.

186 Exogenous LCFAs are not major TCA cycle substrates.

187 One possible explanation for the minor contribution of palmitate-derived carbons to TCA cycle
188 metabolites is that there are differences in the utilisation of FAs based upon saturation (double
189 bonds) and carbon chain lengths. Palmitate (FA 16:0) was chosen first because it is the most
190 abundant circulating FA in humans[24]. Thus, we set out to test other LCFA species. Cells were
191 incubated in media containing physiological levels of glucose and glutamine, supplemented
192 with [U-^{13}C]-palmitate (FA 16:0), stearate (FA 18:0), oleate (FA 18:1), linoleate (FA 18:2), or
193 linolenate (FA 18:3). Each ^{13}C-FA enriched their direct acyl-carnitine counterpart species by a
194 fractional ratio of 0.5-0.95 (Figure 4A). Consistent with the results of our palmitate tracing
195 experiments, exogenous LCFAs contributed <10% of labelled carbons to citrate, oxoglutarate,
196 or malate (Figure 4B). Interestingly, cell lines with the smallest FAO shift in activity when
197 deprived of glucose (DO4, HEPG2, MCF-7, and HT-29 cells) had increased enrichments across
198 all labelled FAs to TCA cycle metabolites compared to an unlabelled control (Figure 4B).
199 However, these enrichment patterns (<10%) from LCFAs were substantially less than glucose

200 (30-50%) and glutamine (20-45%) (Figure 2). Collectively, these data further demonstrate that
201 exogenous LCFAs of different saturation and chain lengths are minor carbon sources to the
202 TCA cycle.

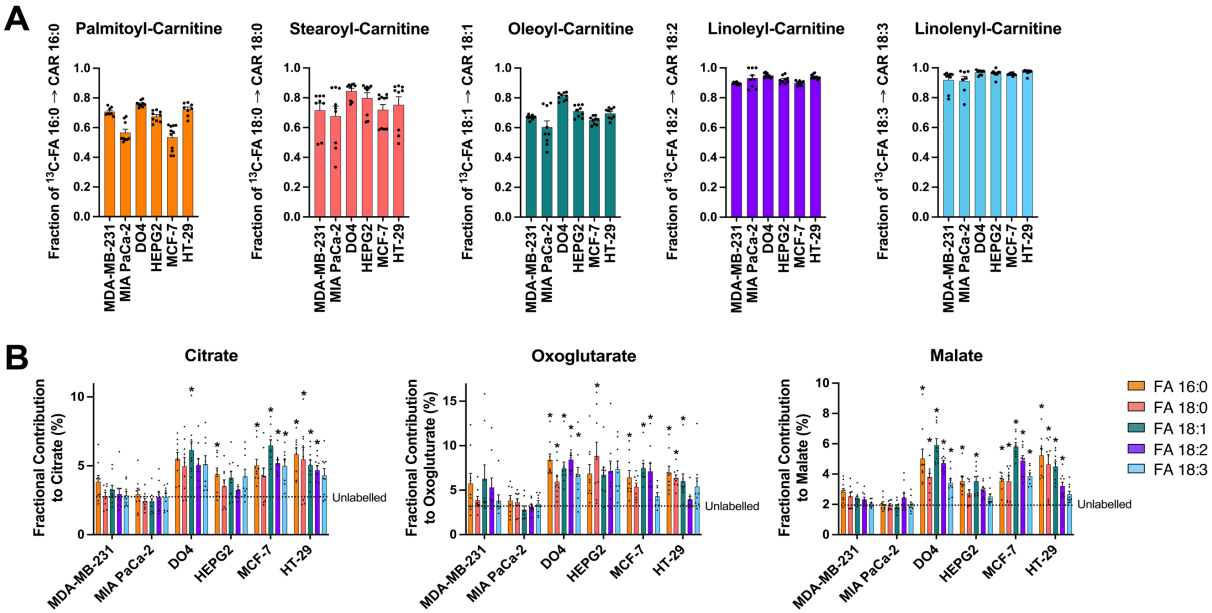

203 **Figure 4. Extracellular LCFAs are minor contributing fuel sources to the TCA cycle in a**
204 **pan-cancer setting.**

205 (A) Fractional contribution of acyl-carnitines associated with the [U-^{13}C]- 16:0, 18:0, 18:1, 18:2, 18:3 substrates.
206 N=9 per cell line.
207 (B) Fractional contribution of [U-^{13}C]-FA to citrate, oxoglutarate, malate. N=9 per cell line.

208 Graphs show mean ± SEM unless stated otherwise. P<0.05 by One-way ANOVA with Dunnett's multiple
209 comparisons test, *compared to unlabelled control (dotted line). See also Figure S4.

210 LCFAs are incompletely oxidised in cancer cells.

211 We observed substantial labelling from exogenous LCFAs directly into acyl-carnitines but a
212 minimal utilisation by the TCA cycle, and next questioned if this could be explained incomplete
213 oxidation of LCFAs to acetyl-CoA. Our results support this hypothesis by showing FA 16:0,
214 18:0, and 18:1 greatly enrich shortened acyl-carnitine species (Figure 5), a known read-out of
215 incomplete FAO[25,26]. Specifically, in all cancer cells, FA 16:0 enriched CAR 14:0 to CAR 12:0,
216 FA 18:0 enriched CAR 16:0 to CAR 12:0, and FA 18:1 enriched CAR 16:1 to CAR 12:1 (Figure
217 5). Together, these data provide evidence that LCFAs are not completely oxidised to the
218 maximal amount of acetyl-CoA for the TCA cycle. We propose that this evidence of enriched

shorted acyl-carnitine species from exogenous LCFAs could explain the minimal contribution of LCFA-derived carbons to the TCA cycle in cancer cells as the maximal amount of acetyl-CoA resulting from complete FAO is not reached.

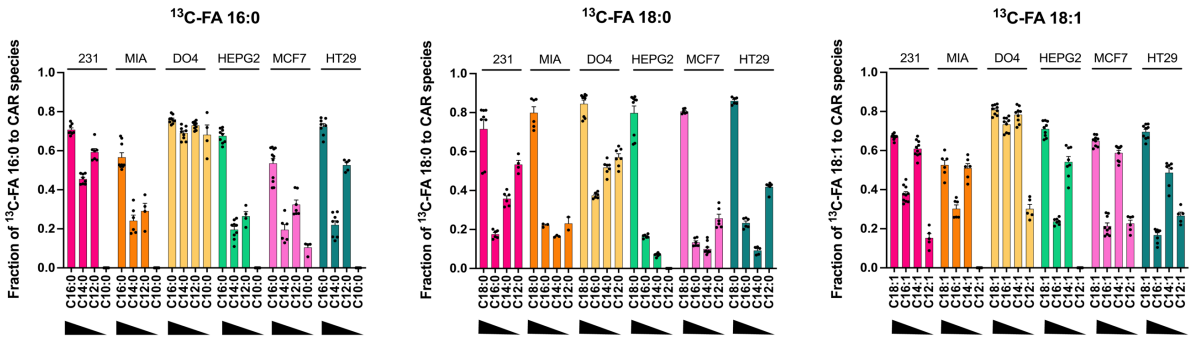

Figure 5. LCFAs undergo incomplete FAO.

Fractional contributions of [U-^{13}C]-FA 16:0, 18:0, 18:2 to shorter chain acyl-carnitine species. N=9 per cell line. Graphs show mean ± SEM.

226 # Discussion

227 Although the convergence of glucose and glutamine at the TCA cycle has been a significant
228 focus of the mitochondrial metabolism field in cancer, the contribution of FAO to the TCA
229 cycle remains underappreciated. Here, we show that exogenous LCFAs were minor carbon
230 sources to the TCA cycle compared to glucose and glutamine, irrespective of the FAO capacity
231 of cancer cells, and this could be explained by the occurrence of incomplete oxidation.

232 Cancer cell metabolism is highly adaptable under nutrient-deprived conditions and can switch
233 to alternative fuel sources to maintain tumour survival[27]. Notably, previous studies observed
234 cells that are highly glycolytic can also upregulate FAO as a partial compensatory measure
235 when glucose uptake is limited or deprived to maintain OXPHOS and ATP production[21,23]. Our
236 results support these phenomena as we showed that cancer cells undergo a metabolic shift to
237 increase FAO rates and the contribution of palmitate to the TCA cycle and cataplerosis
238 metabolites when deprived of glucose and glutamine. These results were in striking contrast to
239 the minor carbon fuelling from LCFAs to the TCA cycle in glucose and glutamine replete
240 conditions. However, this adaptive role in fuelling the TCA cycle could not meet the levels
241 sustained by glucose or glutamine, and most importantly, the TCA cycle metabolite pool sizes
242 were markedly reduced in substrate-deprived settings. These results show that FAO is an
243 insufficient carbon source to maintain TCA cycle activity and that this has no relationship to
244 the intrinsic dynamic FAO capacity of cancer cells.

245 Others have shown that inhibiting CPT1a, the initiating step for LCFA entry to the
246 mitochondria, leads to decreased respiration and cell viability[9-12,28]. The primary assumption
247 made by these studies is that mitochondrial LCFAs are solely destined to undergo complete
248 oxidation within the mitochondria and provide acetyl-CoA for the TCA cycle, and subsequent
249 ATP production to support tumour growth. These studies presumptively couple CPT1a activity

250 to FAO and bioenergetics. A key example is a study that combined glycolysis and CPT1a
251 inhibitors that synergistically improved survival in a glioblastoma model and concluded that
252 co-targeting of glycolysis and FAO is a new therapeutic strategy[21]. Our findings demonstrated
253 here and in our recent study[19], directly challenge these assumptions by showing that LCFAs
254 are a minor carbon source to the TCA cycle. A logical explanation for this lack of effect was
255 that LCFAs entering the mitochondria via CPT1a are not completely oxidised for the TCA
256 cycle, nor are the sole intra-mitochondrial fate as evidenced by enriched shortened acyl-
257 carnitines from LCFAs.

258 Incomplete FAO, evidenced by the production of short and medium even-chained acyl-
259 carnitines, has previously been showed to occur in skeletal muscle in the surplus of fatty
260 acids[26]. Our findings are the first to clearly demonstrate that cancer cells from different lineages
261 also undergo incomplete oxidation of exogenous LCFAs and provide a solid foundation to
262 explore the role of shortened acyl-carnitines for cancer cell survival. In the setting of type 2
263 diabetes mellitus it was shown that there is an accumulation of shortened acyl-carnitines
264 concentrations in the plasma of patients due to incomplete FAO and that this was linked to low
265 levels of LCFA utilization by the TCA cycle[29] to ultimately promote proinflammatory pathways
266 necessary for insulin resistance. Interestingly, results from our pan-cancer study parallel this
267 phenotype of incomplete FAO and minor LCFA carbon contribution to the TCA cycle observed
268 in type 2 diabetic patients. We propose that future investigations into the fates of shortened
269 acyl-carnitines in cancer settings could provide novel insights into the roles of FAs for cancer
270 survival.

271 A limitation of these studies is that we only quantified the contribution of exogenous LCFAs,
272 glucose, and glutamine which totalled 40-80% of the TCA metabolite pools, but other
273 contributing carbon sources were likely at play. We could rule out the potential incorporation

274 of free fatty acids and lipids as we incubated our cells in serum-free medium. However,
275 endogenous FA sources, or amino acids in DMEM tracing medium, like branched chain amino
276 acids, can also contribute carbons to the TCA cycle[30-32].

277 Our study in multiple cancer cells provides quantitative evidence that LCFAs are minor carbons
278 sources to the TCA cycle compared to glucose and glutamine, irrespective of intrinsic FAO
279 activity. Fundamentally, we propose a new model that exogenous LCFAs undergo incomplete
280 oxidation within the mitochondria which challenges the assumption that the TCA cycle is the
281 sole fate of LCFAs entering the mitochondria in cancer cells. We expect that future
282 investigations into the occurrence of incomplete FAO in cancer cells will provide a basis for
283 exploring the role of shortened acyl-carnitines for cancer survival and tumour growth.

284 # Methods

285 ## Key resources table

REAGENT or RESOURCE	SOURCE	IDENTIFIER
Antibodies		
Mouse monoclonal anti-CPT1A	Abcam	Cat#Ab128568; RRID: AB_11141632
Rabbit monoclonal anti-GAPDH	Cell Signalling Technology	Cat#2118; RRID: AB_561053
Chemicals, peptides, and recombinant proteins		
Enzalutamide	Selleckchem	Cat#S1250
Etomoxir	Sigma-Aldrich	Cat#C986W52
Lipofectamine RNAiMAX transfection reagent	Thermo Fisher Scientific	Cat#13778075
[1-^{14}C] Palmitic acid	Perkin Elmer	Cat#NEC075H250UC
Palmitic acid	Sigma-Aldrich	Cat#P0500
D-Glucose	Sigma-Aldrich	Cat#273053
L-Glutamine	Gibco	Cat#25030081
Fatty acid free BSA	Bovogen	Cat#BSAS0.10
L-carnitine hydrochloride	Sigma-Aldrich	Cat#C0283
Mitotracker Green	Thermo Fisher Scientific	Cat#M7514
Mitotracker Red	Thermo Fisher Scientific	Cat#M7512
FCCP	Sigma-Aldrich	Cat#SML2959
DTT	Sigma-Aldrich	Cat#D0632
Protease and Phophatase Inhibitor Cocktail, EDTA free	Astral Scientific	Cat#T-2496
Thiazolyl blue tetrazolium bromide MTT reagent	Sigma-Aldrich	Cat#M2128
Linoleic acid	Sigma Aldrich	Cat#L1012
D-Glucose (U-13C6, 99%)	Cambridge Isotope Laboratories, Inc.	Cat#CLM-1396
L-Glutamine (U-13C5, 99%)	Cambridge Isotope Laboratories, Inc.	Cat#CLM-1822-H
Palmitic acid (U-13C16, 98%)	Cambridge Isotope Laboratories, Inc.	Cat#CLM-409
Stearic acid (U-13C18, 98%)	Cambridge Isotope Laboratories, Inc.	Cat#CLM-6990
Linoleic acid (U-13C18, 98%)	Cambridge Isotope Laboratories, Inc.	Cat#CLM-10487
Linolenic acid (U-13C18, 98%)	Cambridge Isotope Laboratories, Inc.	Cat#8386
Critical commercial assays		
Pierce BCA Protein assay kit	Thermo Fisher Scientific	Cat#23225
Immobilon Crescendo Western HRP substrate	Merck Millipore	Cat#WBLUR0500
Experimental models: Cell lines		
MDA-MB-231	ATCC	ATCC HTB-26 RRID: CVCL_0062
MDA-MB-468	ATCC	ATCC HTB-132
MCF7	ATCC	ATCC HTB-22
MDA-MB-134	ATCC	ATCC HTB-23
C4-2B	ATCC	ATCC CRL-3315
PC-3	ATCC	ATCC CRL-1435

22Rv1	ATCC	ATCC CRL-2505 RRID: CVCL_1045
LNCaP	ATCC	ATCC CRL-1740 RRID: CVCL_1379
DU145	A/Prof. Luke Selth, Flinders University	ATCC HTB-81
CWR-AD1	A/Prof. Luke Selth, Flinders University	Nyquist 2013[33], Li 2013[34]
MR42D	Prof. Lisa Butler, SAHMRI	Bishop 2017[35]
HEPG2	A/Prof. Susan McLennan, University of Sydney	Nagarajan 2019[36]
Ishikawa	Prof. Kyle Hoehn, UNSW	RRID: CVCL_2529
MFE296	Prof. Kyle Hoehn, UNSW	RRID: CVCL_1406
MFE319	Prof. Kyle Hoehn, UNSW	RRID: CVCL_2112
U87	Prof. Lenka Munoz, University of Sydney	RRID: CVCL_3429
MIAPACA-2	A/Prof Thomas Grewal, University of Sydney	RRID: CVCL_0428
OVCAR3	A/Prof. David Croucher, Garvan Institute	RRID: CVCL_0465
SKOV3	A/Prof. David Croucher, Garvan Institute	RRID: CVCL_0532
A375	Dr. Lorey Smith, Peter MacCallum Cancer Centre	ATCC CRL-1619 RRIDL CVCL_0132
HT144	Dr. Lorey Smith, Peter MacCallum Cancer Centre	ATCC HTB-63 RRID: CVCL_0318
WM266.4	Dr. Lorey Smith, Peter MacCallum Cancer Centre	ATCC CRL-1676 RRID: CVCL_2765
DO4-M1	Dr. Lorey Smith, Peter MacCallum Cancer Centre	Parmenter 2014[37]
Detroit562	A/Prof Thomas Grewal, University of Sydney	RRID: CVCL_1171
HT29	A/Prof. Kellie Charles, University of Sydney	RRID: CVCL_A8EZ
SW-48	A/Prof. Kellie Charles, University of Sydney	RRID: CVCL_1724
SW-1417	A/Prof. Kellie Charles, University of Sydney	RRID: CVCL_1717
Software and algorithms		
GraphPad Prism V9	GraphPad Software	https://www.graphpad.com/
Image Lab 6.1	Bio-Rad	https://www.bio-rad.com/en-au/product/image-lab-software
FlowJo 2	FlowJo LLC	https://www.flowjo.com/
MATLAB	Mathworks	https://au.mathworks.com/products/matlab.html
MSConvert	N/A	Chambers 2012[38]
MSDial	Riken	http://prime.psc.riken.jp/compms/msdial/main.html
Biorender	Biorender	https://biorender.com/

286

287

288 # Method details

289 **Cell lines and culture conditions**

290 A panel of 27 adherent cancer cell lines from 10 different origins were used in this study. Cell
291 lines were obtained both from vendors and kindly provided by academic labs. Details of
292 culturing media (Gibco) can be found in Supp Table 1. All culturing media were supplemented
293 with 10% fetal bovine serum (Cytiva Hyclone) and 1% penicillin/streptomycin (Gibco). Cells
294 were incubated at 37°C and 5% CO_2.

295 **^{14}C-Radiolabelling**

296 Cells were seeded in technical triplicates in 6-well plates. The next day, the cells were washed
297 in warm PBS and incubated in 600 μL media containing 0.1 mmol/L cold palmitate, [1-^{14}C]
298 palmitate (0.1 μCi/mL; Perkin Elmer) conjugated to 2% (wt/vol) FA-free BSA and 1 mmol/L
299 -carnitine in RPMI or DMEM glucose-free medium (Gibco) for 4 hours. Fatty acid oxidation
300 rates were determined from CO_2 production as previously described[19] in either 0 mM or 5 mM
301 glucose to measure FAO flexibility. Protein content was measured by BCA protein assay and
302 absorbances read at 540 nm using a Tecan infinite M1000 pro plate reader.

303 **Radiolabelled glucose titration**

304 MDA-MB-231 cells were treated as above for radiolabelled experiments, supplemented with
305 0, 1, 3, 5, 7, 9 11, 25 mM glucose +/- 10 μM etomoxir. In the selected panel of 6 cell lines,
306 cells were treated as above for radiolabelled experiments, supplemented with 0, 1, 3, 5 mM
307 glucose.

308 **Mitotracker**

309 Cells were seeded in 12-well plates at a density of $2x10^5$ cells/well in RPMI or DMEM HG
310 medium. After 24 hours, cells were washed in warm PBS and obtained by trypsinisation and
311 collected in serum-free RPMI medium. The cell suspension was centrifuged at 1500 rpm for

312 5min in fluorescence-activated cell sorting (FACS) tubes. Cells were subsequently stained with
313 200nM Mitotracker Red and Mitotracker Green at 37°C for 30 mins. Additionally, unstained,
314 red only, green only, and 2.5mM FCCP treated cells were included as experimental controls.
315 Cells were centrifuged at 1500 rpm for 5min and fixed with 4% paraformaldehyde at 37°C for
316 10 mins. Cells were washed with warm PBS and centrifuged at 1500 rpm for 5 mins and
317 resuspended in 150 mL PBS before the samples were read on a BD LSR Fortessa flow
318 cytometer. Data analysis was performed using FlowJo software.

319 **Immunoblotting**

320 Cells were seeded in 6-well plates ($5x10^5$). After 24 hours, cells were lysed in RIPA buffer
321 containing 1% DTT and 0.1% protease and phosphatase inhibitor cocktail. Protein content was
322 measured by BCA protein assay, and absorbances were read at 540 nm using a TECAN infinite
323 M1000 pro plate reader. Cell lysates were subjected to SDS-PAGE, and transferred to
324 polyvinylidene difluoride (PVDF) membranes (Merck Millipore). Ponceau staining was
325 performed on membranes as a loading control, and then membranes were immunoblotted for
326 CPT1a. Chemiluminescence was performed using Luminata Crescendo Western HRP
327 Substrate and imaged using the Bio-Rad ChemiDoc MP Imaging System and Image Lab
328 software 4.1 (Bio-Rad Laboratories).

329 **Cell viability**

330 Cells were seeded in 96-well plates in 6 well replicates ($3x10^3$ cells/well). After 24 hours the
331 media was removed and replaced with glucose- and glutamine free media (Gibco)
332 supplemented with 5 mM glucose, 1 mM glutamine and/or 150 μM FAs, conjugated to 2%
333 (wt/vol) FA-free BSA. For glucose-deprived conditions, DMEM no glucose, no glutamine
334 media was supplemented with 1 mM glutamine and 150 mM palmitate; for glucose and
335 glutamine-deprived conditions, media was supplemented with 150 μM palmitate only. Media

336 supplemented with 10% FBS was used as a control. At 6, 12 and 24 hours, 50 mL of MTT
337 reagent was added to wells. MTT reactions were incubated at 37°C and 5% CO_2 for 4 hours,
338 and then stopped by replacing media with 100mL DMSO (Sigma–Aldrich) per well.
339 Absorbances were read at 540 nm using a TECAN infinite M1000 pro plate reader. Cells were
340 seeded in 6-well plates at $5x10^5$ cells/well for live cell counts. After 24 hours, media was
341 replaced as described for the MTT assay, and cells counted by Trypan blue (Gibco) exclusion
342 at 6 and 24 hours.

343 **[U-^{13}C]-stable isotope tracing**

344 Cells were seeded in 6-well plates ($5x10^5$). After 24 hours, plates were washed with warm PBS
345 and media replaced with 600μL of DMEM no glucose, no glutamine media (Gibco)
346 supplemented with 5 mM glucose, 1 mM glutamine and/or 150 μM FAs, replaced with their
347 respective [U-^{13}]-C forms. [U-^{13}C]-FAs (Palmitate (16:0), Oleate (18:0), Stearate (18:1),
348 Linoleate (18:2), or Linolenate (18:3). For glucose-deprived conditions DMEM no glucose, no
349 glutamine media was supplemented with 1mM glutamine and [U-^{13}C]-150 μM palmitate; for
350 glucose and glutamine-deprived conditions media was supplemented with [U-^{13}C]-150 μM
351 palmitate only. FAs were conjugated to 2% (wt/vol) FA-free BSA-containing media for 24
352 hours at 37°C before treating cells. Cells were incubated in ^{13}C containing medium for 6 hours.

353 **Extracellular substrate sampling**

354 Cells were seeded in 6-well plates ($5x10^5$). After 24 hours, wells were washed with warm PBS
355 and media replaced with 1 mL or 2 mL of DMEM with no glucose, no glutamine media
356 supplemented with 5 mM glucose, 1 mM glutamine, and 150 μM FAs, conjugated to 2%
357 (wt/vol) FA-free BSA. 100 μL of extracellular media were collected from wells at 3, 6, 12, 24
358 hour timepoints for cells incubated in 1mL of media, and 12, 24 hours for cells incubated in 2

359 mL of media. Media samples were centrifuged at 16,000 x g for 5 mins at 4°C, and the
360 supernatant collected for subsequent LC-MS analysis.

361 **Cell lysate extraction for LC-MS**

362 Media was aspirated from plates and the cells washed with 2 mL ice-cold 0.9% (w/v) NaCl.
363 Cells were scraped with 300 μL of extraction buffer, EB, (1:1 LC/MS methanol:water (Optima)
364 + 0.1x internal standards (non-endogenous polar metabolites) and transferred to a 1.5 mL
365 microcentrifuge tube. A further 300 μl of EB was added to the cells and combined in the tube.
366 600 μL of chloroform (Honeywell) was added before vortexing and incubating on ice for 10
367 mins. Tubes were vortexed briefly and centrifuged at 15,000g for 10 mins at 4°C. The aqueous
368 upper layer was collected and dried without heat using a Savant SpeedVac (Thermo Fisher) for
369 metabolomics LC-MS analysis. The lower layer was collected and dried under nitrogen flow
370 for lipidomics LC-MS analysis.

371 **Measuring stable-isotope labelled metabolites by LC-MS**

372 Dried aqueous upper phase samples were resuspended in 40 mL Amide buffer A (20mM
373 ammonium acetate, 20 mM ammonium hydroxide, 95:5 HPLC H_2O: Acetonitrile (v/v)) and
374 vortexed and centrifuged at 15,000g for 5 mins at 4°C. 20 mL of supernatant was transferred
375 to HPLC vials containing 20 mL acetonitrile for LCMS analysis of amino acids and glutamine
376 metabolites. The remaining 20 mL of the resuspended sample was transferred to HPLC vials
377 containing 20 mL LC-MS H_2O for LCMS analysis of glycolytic, pentose phosphate pathway,
378 and TCA cycle metabolites. Amino acids and glutamine metabolites were measured using
379 Vanquish-TSQ Altis (Thermo) LC-MS/MS system. Analyte separation was achieved using a
380 Poroshell 120 HILIC-Z Column (2.1x150 mm, 2.7 mm) (Agilent) at ambient temperature. The
381 pair of buffers used were Amide buffer A and 100% acetonitrile (Buffer B), flowed at 200
382 mL/min; injection volume of 5 mL. Glycolytic, pentose phosphate pathway and TCA cycle

383 metabolites were measured using 1260 Infinity (Agilent)-QTRAP6500+ (AB Sciex) LC-
384 MS/MS system. Analyte separation was achieved using a Synergi 2.5 mm Hydro-RP 100A LC
385 Column (100x2 mm) at ambient temperature. The pair of buffers used were 95:5 (v/v)
386 water:acetonitrile containing 10 mM tributylamine and 15 mM acetic acid (Buffer A) and 100%
387 acetonitrile (Buffer B), flowed at 200 mL/min; injection volume of 5 mL. Raw data from both
388 LC-MS/MS systems were extracted using MSConvert[38] and in-house MATLAB scripts.

389 **Measuring extracellular substrates by LC-MS**

390 20 μL of collected extracellular media was mixed with 80 μL water, vortexed. 10 μL of diluted
391 media was mixed with 90 μL of extraction buffer containing 1:1 (v/v) acetonitrile and methanol
392 + 1x internal standards (non-endogenous standards) at -30°C. The mixture was centrifuged at
393 12,000xg for 5 min at 4°C and transferred into HPLC vials for LC-MS analysis measured using
394 the Vanquish-TSQ Altis as described above. Raw data from both LC-MS/MS systems were
395 extracted using MSConvert[38] and in-house MATLAB scripts.

396 **Measuring stable isotope labelled lipids by LC-MS**

397 Dried lower phase samples were resuspended in 100 μL 4:2:1 (v/v)
398 isopropanol:methanol:chloroform containing 7.5 mM ammonium formate. Acyl-carnitine
399 lipids were measured using a Thermo Scientific Q-Exactive-HF-X Hybrid Quadrupole
400 Orbitrap LC-MS/MS system. Analyte separation was achieved using an Agilent Poroshell 120,
401 HILIC, 2.1x100 mm, 2.7 μm column. The pair of buffers used were 0.1(v/v)% formic acid and
402 10 mM ammonium formate in H_2O and 0.1(v/v)% formic acid in acetonitrile, flowed at 200
403 μL/min on positive mode. MS1 data was acquired with the following settings: 3.5 kV,
404 capillarity temperature 300°C, 120,000, injection time 100 ms, AGC $1x10^6$, scan range 200-
405 1000. For ddMS2 data acquirement, the following settings were used: top 5, resolution 30,000,
406 200-2000, isolation 1.0m/z, nce 30, AGC target $1x10^3$, intensity threshold $5x10^3$, dynamic

407 exclusion 20s. Raw data from both LC-MS/MS systems were extracted using MSConvert[38]
408 and in-house MATLAB scripts.

409 **Quantification and statistical analysis**

410 Student's t-test, one- or two-way ANOVA with Dunnett's or Tukey's multiple comparisons,
411 and linear regression statistical tests were performed with GraphPad Prism 9.0 (GraphPad
412 Software). $P < 0.05$ was considered significant. Data are reported as mean ± standard error of
413 the mean (SEM), standard deviation (SD), or min-max values of at least three independent
414 determinations. Radiolabelling experiments for the expansive cell line panel were of at least
415 one independent determination (N=1-x as indicated in the respective figure legend) with at
416 least 3 technical replicates each. Schematic diagrams were created with Biorender.com.

417 # Supplementary information

418 ## Supplementary Table 1: Cell line details

Cell line	Cancer type	Culture media (Gibco)
MDA-MB-231	Breast	DMEM HG
MDA-MB-468		RPMI
MCF7		DMEM HG
MDA-MB-134		RPMI
C4-2B	Prostate	RPMI
PC-3		RPMI
22Rv1		RPMI
LNCaP		RPMI
DU145		RPMI
CWR-AD1		RPMI
MR42D		RPMI + 10µM enzalutamide
HEPG2	Liver	DMEM HG
Ishikawa	Endometrial	DMEM HG
MFE296		DMEM HG
MFE319		DMEM HG
U87	Glioblastoma	DMEM HG
MIAPACA-2	Pancreatic	DMEM HG
OVCAR3	Ovarian	RPMI
SKOV3		RPMI
A375	Melanoma	RPMI
HT144		RPMI
WM266.4		RPMI
DO4-M1		RPMI
Detroit562	Head and Neck	DMEM/F12
HT29	Colorectal	DMEM HG
SW-48		DMEM HG
SW-1417		DMEM HG

419

420

Supplementary figures

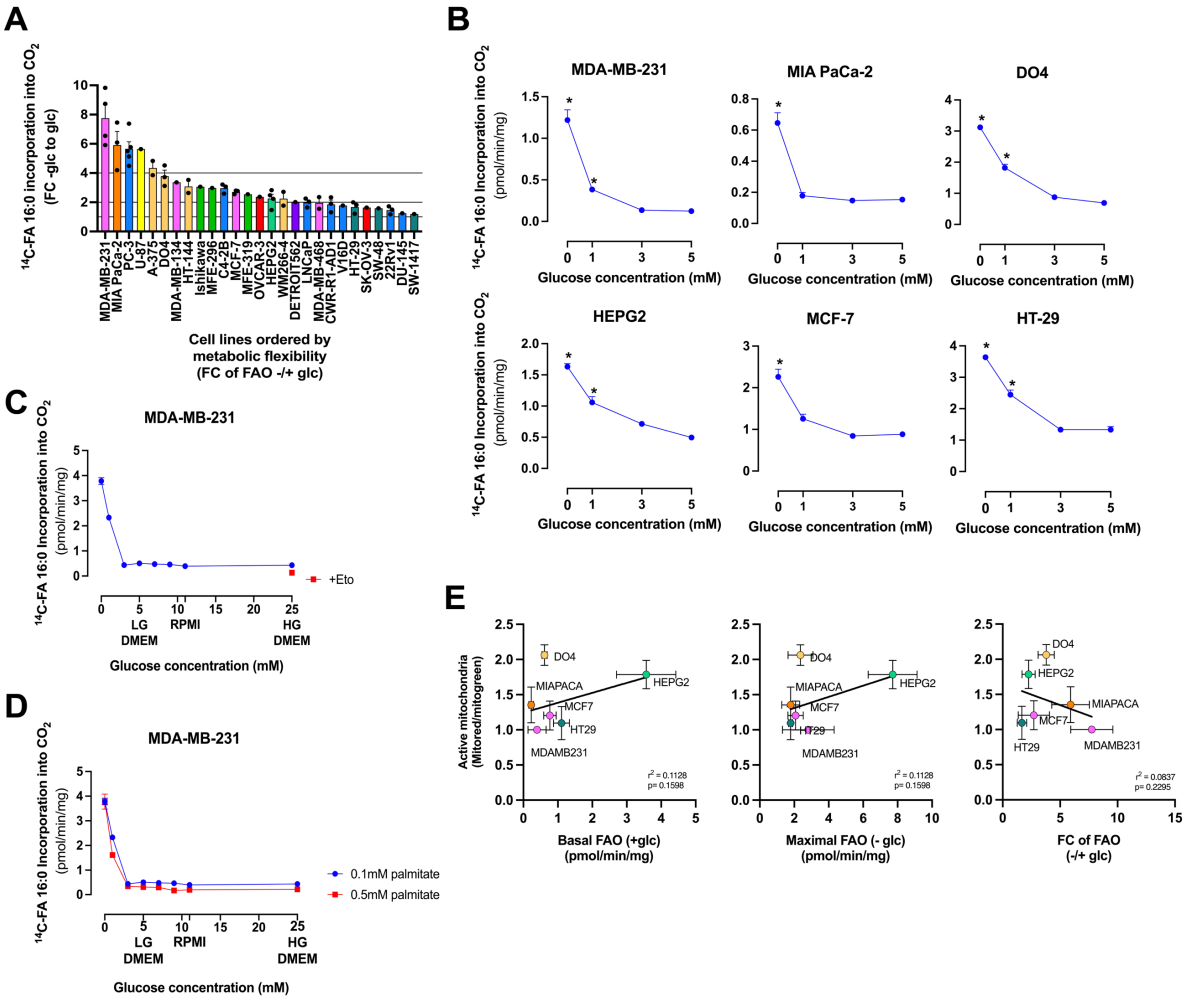

Figure S1, related to figure 1. FAO increases most dramatically under complete glucose deprivation.

(A) Fold change (FC) difference of ^{14}C-FA 16:0 oxidation rates -/+ glucose. Cell lines ranked by fold change difference magnitude. N=1-5 per cell line.
(B) [1-^{14}C]-FA 16:0 oxidation rates in the presence of 5 mM, 3 mM, 1 mM, or 0 mM glucose. N=3 per cell line. Statistically significant differences to ^{14}C-FA 16:0 oxidation experiments in 5mM glucose shown.
(C) [1-^{14}C]-FA 16:0 oxidation rates in MDA-MB-231 cells in the presence of 0 to 25 mM glucose +/- etomoxir in 0.1mM ^{14}C-FA 16:0. N=1, 3 technical replicates.
(D) [1-^{14}C]-FA 16:0 oxidation rates in MDA-MB-231 cells in the presence of 0 to 25 mM glucose +/- etomoxir in 0.1mM ^{14}C-FA 16:0 compared to 0.5 mM ^{14}C-FA 16:0. N=1, 3 technical replicates.
(E) Correlations between active mitochondria content and basal (+glc), maximal (-glc), and fold change (-/+) FAO rates. N=3 per cell line.

Graphs show mean ± SEM. *p<0.05 by One-way ANOVA with Dunnett's multiple comparisons test.

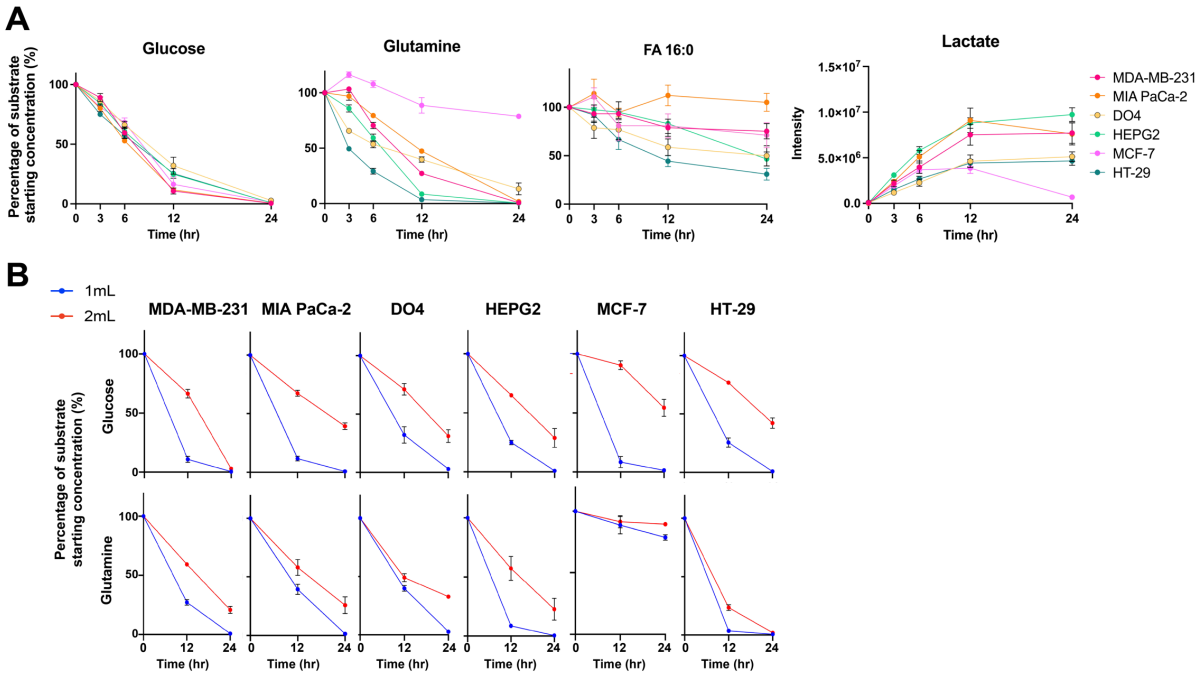

436 **Figure S2, related to figure 2. Substrate uptake and production of cancer cells over 24**
437 **hours.**

438 (A) Percentage of substrate starting concentration glucose, glutamine, and FA 16:0, and intensity of lactate
439 uptake over 24 hours. N=3 per cell line.
440 (B) Percentage of substrate starting concentration glucose or glutamine at 1 mL (blue) or 2 mL (red) medium.
441 N=3 per cell line.
442 Graphs show mean ± SEM.

443

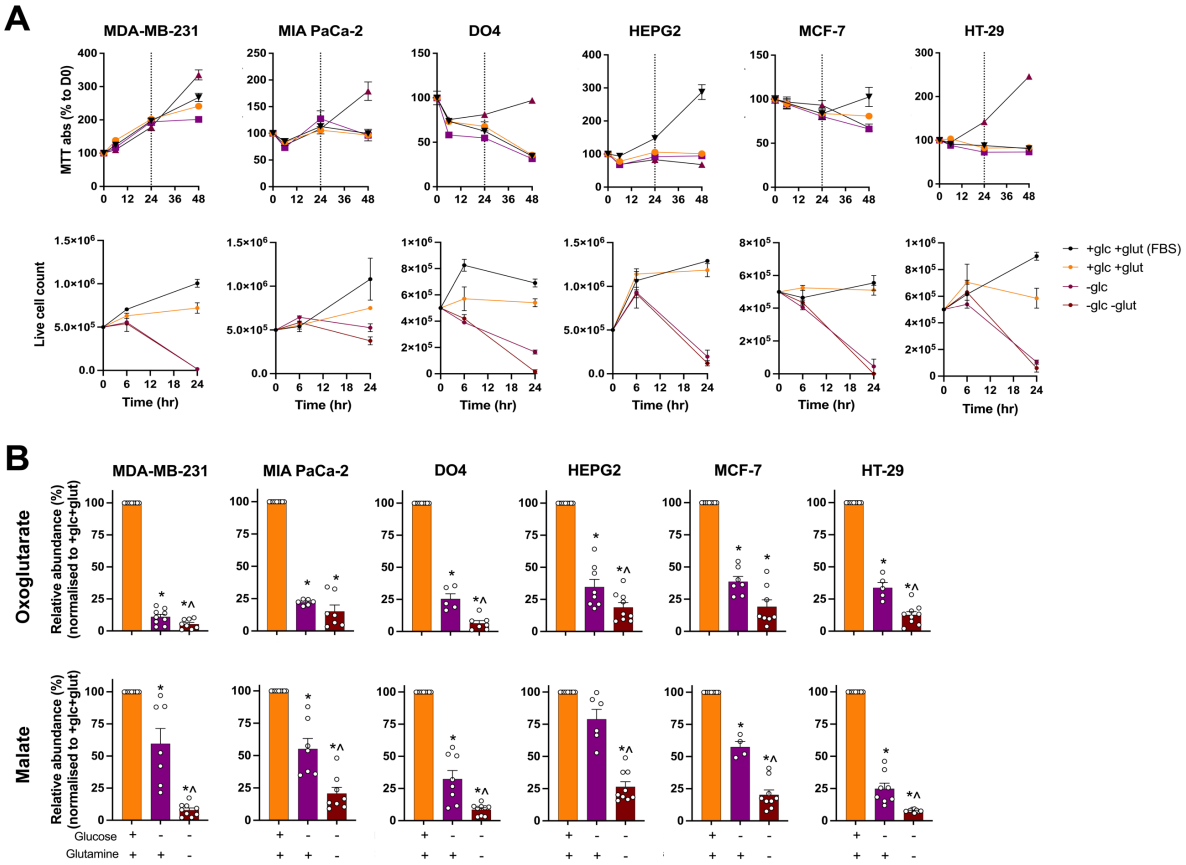

Figure S3, related to figure 3. Palmitate cannot completely maintain TCA cycle activity under glucose and glutamine deprivation.

(A) Impact of glucose- or glucose and glutamine- deprivation on metabolic activity (top) assessed by MTT assay absorbance results to 48hours normalised to day 0 results (Dotted line at 24 hours indicates replenishment of media); or Cell viability (bottom) assessed by live cell counts at 0, 6 and 24 hours normalised to day 0 results. N=3 per group.

(B) Relative abundance (normalised to +glucose/+glutamine) of [U-^{13}C]-FA 16:0 to oxoglutarate or malate. N=5-9 per cell line.

Graphs show mean ± SEM. P<0.05 by One-way ANOVA with Dunnett's multiple comparisons test. *compared to +glucose/+glutamine, ^compared to -glucose/+glutamine

Acknowledgements

N.T.S. is supported by the Australian Rotary Health/Rotary Club of Blacktown City 'Mel Grey' PhD scholarship. A.J.H. is supported by a Robinson Fellowship from the University of Sydney. This work was supported by funding from The University of Sydney. We thank the Sydney Mass Spectrometry facility for access to LC-MS instruments; Dr Helen McGuire and the Sydney Cytometry core facility for assistance with mitotracker experiments; and all collaborators who kindly donated cell lines specified in the key resources table.

Author contributions

Conceptualisation by A.J.H. and L.E.Q. Project administration, visualisation, writing-original draft by N.T.S. Investigation by N.T.S., M.F.H.S., M.G., and A.W. Methodology by L.E.Q. Software by N.T.S., and L.E.Q. Formal analysis by N.T.S and L.E.Q. Writing-editing & reviewing by N.T.S., L.E.Q., and A.J.H. Funding acquisition, resources by A.J.H. Supervision by A.J.H., and L.E.Q.

Declaration of interests

The authors declare that they have no competing interests.

470 # References:

471 1. Lin, H., Patel, S., Affleck, V.S., Wilson, I., Turnbull, D.M., Joshi, A.R., Maxwell, R.,
472 and Stoll, E.A. (2017). Fatty acid oxidation is required for the respiration and
473 proliferation of malignant glioma cells. Neuro Oncol. *19*, 43-54.
474 10.1093/neuonc/now128.

475 2. Nassar, Z.D., Mah, C.Y., Dehairs, J., Burvenich, I.J., Irani, S., Centenera, M.M.,
476 Helm, M., Shrestha, R.K., Moldovan, M., Don, A.S., et al. (2020). Human DECR1 is
477 an androgen-repressed survival factor that regulates PUFA oxidation to protect
478 prostate tumor cells from ferroptosis. Elife *9*. 10.7554/eLife.54166.

479 3. Padanad, M.S., Konstantinidou, G., Venkateswaran, N., Melegari, M., Rindhe, S.,
480 Mitsche, M., Yang, C., Batten, K., Huffman, K.E., Liu, J., et al. (2016). Fatty Acid
481 Oxidation Mediated by Acyl-CoA Synthetase Long Chain 3 Is Required for Mutant
482 KRAS Lung Tumorigenesis. Cell Rep. *16*, 1614-1628. 10.1016/j.celrep.2016.07.009.

483 4. Lee, J.-S., Oh, S.-J., Choi, H.-J., Kang, J.H., Lee, S.-H., Ha, J.S., Woo, S.M., Jang, H.,
484 Lee, H., and Kim, S.-Y. (2020). ATP Production Relies on Fatty Acid Oxidation
485 Rather than Glycolysis in Pancreatic Ductal Adenocarcinoma. Cancers (Basel) *12*,
486 2477.

487 5. Samudio, I., Harmancey, R., Fiegl, M., Kantarjian, H., Konopleva, M., Korchin, B.,
488 Kaluarachchi, K., Bornmann, W., Duvvuri, S., Taegtmeyer, H., and Andreeff, M.
489 (2010). Pharmacologic inhibition of fatty acid oxidation sensitizes human leukemia
490 cells to apoptosis induction. J. Clin. Invest. *120*, 142-156. 10.1172/jci38942.

491 6. Fritz, I.B., and Yue, K.T. (1963). LONG-CHAIN CARNITINE
492 ACYLTRANSFERASE AND THE ROLE OF ACYLCARNITINE DERIVATIVES
493 IN THE CATALYTIC INCREASE OF FATTY ACID OXIDATION INDUCED BY
494 CARNITINE. J. Lipid Res. *4*, 279-288.

495 7. Melone, M.A.B., Valentino, A., Margarucci, S., Galderisi, U., Giordano, A., and
496 Peluso, G. (2018). The carnitine system and cancer metabolic plasticity. Cell Death
497 Dis. *9*, 228. 10.1038/s41419-018-0313-7.

498 8. Qu, Q., Zeng, F., Liu, X., Wang, Q.J., and Deng, F. (2016). Fatty acid oxidation and
499 carnitine palmitoyltransferase I: emerging therapeutic targets in cancer. Cell Death
500 Dis. *7*, e2226-e2226. 10.1038/cddis.2016.132.

501 9. Pike, L.S., Smift, A.L., Croteau, N.J., Ferrick, D.A., and Wu, M. (2011). Inhibition of
502 fatty acid oxidation by etomoxir impairs NADPH production and increases reactive
503 oxygen species resulting in ATP depletion and cell death in human glioblastoma cells.
504 Biochim Biophys Acta *1807*, 726-734. 10.1016/j.bbabio.2010.10.022.

505 10. Schlaepfer, I.R., Rider, L., Rodrigues, L.U., Gijón, M.A., Pac, C.T., Romero, L.,
506 Cimic, A., Sirintrapun, S.J., Glodé, L.M., Eckel, R.H., and Cramer, S.D. (2014). Lipid
507 Catabolism via CPT1 as a Therapeutic Target for Prostate Cancer. Mol. Cancer Ther.
508 *13*, 2361-2371. 10.1158/1535-7163.mct-14-0183.

11. Tirado-Vélez, J.M., Joumady, I., Sáez-Benito, A., Cózar-Castellano, I., and Perdomo, G. (2012). Inhibition of fatty acid metabolism reduces human myeloma cells proliferation. PLoS One *7*, e46484. 10.1371/journal.pone.0046484.

12. Lin, H., Patel, S., Affleck, V.S., Wilson, I., Turnbull, D.M., Joshi, A.R., Maxwell, R., and Stoll, E.A. (2016). Fatty acid oxidation is required for the respiration and proliferation of malignant glioma cells. Neuro Oncol. *19*, 43-54. 10.1093/neuonc/now128.

13. Yao, C.-H., Liu, G.-Y., Wang, R., Moon, S.H., Gross, R.W., and Patti, G.J. (2018). Identifying off-target effects of etomoxir reveals that carnitine palmitoyltransferase I is essential for cancer cell proliferation independent of β-oxidation. PLoS Biol. *16*, e2003782. 10.1371/journal.pbio.2003782.

14. O'Connor, R.S., Guo, L., Ghassemi, S., Snyder, N.W., Worth, A.J., Weng, L., Kam, Y., Philipson, B., Trefely, S., Nunez-Cruz, S., et al. (2018). The CPT1a inhibitor, etomoxir induces severe oxidative stress at commonly used concentrations. Sci. Rep. *8*, 6289. 10.1038/s41598-018-24676-6.

15. Carracedo, A., Cantley, L.C., and Pandolfi, P.P. (2013). Cancer metabolism: fatty acid oxidation in the limelight. Nat. Rev. Cancer *13*, 227-232. 10.1038/nrc3483.

16. Martínez-Reyes, I., and Chandel, N.S. (2020). Mitochondrial TCA cycle metabolites control physiology and disease. Nat Commun *11*. 10.1038/s41467-019-13668-3.

17. Shiratori, R., Furuichi, K., Yamaguchi, M., Miyazaki, N., Aoki, H., Chibana, H., Ito, K., and Aoki, S. (2019). Glycolytic suppression dramatically changes the intracellular metabolic profile of multiple cancer cell lines in a mitochondrial metabolism-dependent manner. Sci. Rep. *9*, 18699. 10.1038/s41598-019-55296-3.

18. Yang, L., Moss, T., Mangala, L.S., Marini, J., Zhao, H., Wahlig, S., Armaiz-Pena, G., Jiang, D., Achreja, A., Win, J., et al. (2014). Metabolic shifts toward glutamine regulate tumor growth, invasion and bioenergetics in ovarian cancer. Mol. Syst. Biol. *10*, 728. https://doi.org/10.1002/msb.20134892.

19. Nancy, T.S., Mariam, F.H.-S., Anabel, W., Lisa, M.B., Lake-Ee, Q., and Andrew, J.H. (2024). CPT1a regulates the delivery of extracellular fatty acids for cardiolipin turnover in prostate cancer cells. bioRxiv, 2024.2001.2016.575611. 10.1101/2024.01.16.575611.

20. Balaban, S., Nassar, Z.D., Zhang, A.Y., Hosseini-Beheshti, E., Centenera, M.M., Schreuder, M., Lin, H.-M., Aishah, A., Varney, B., Liu-Fu, F., et al. (2019). Extracellular Fatty Acids Are the Major Contributor to Lipid Synthesis in Prostate Cancer. Mol. Cancer Res. *17*, 949-962. 10.1158/1541-7786.Mcr-18-0347.

21. Kant, S., Kesarwani, P., Prabhu, A., Graham, S.F., Buelow, K.L., Nakano, I., and Chinnaiyan, P. (2020). Enhanced fatty acid oxidation provides glioblastoma cells metabolic plasticity to accommodate to its dynamic nutrient microenvironment. Cell Death Dis. *11*, 253. 10.1038/s41419-020-2449-5.

22. van Weverwijk, A., Koundouros, N., Iravani, M., Ashenden, M., Gao, Q., Poulogiannis, G., Jungwirth, U., and Isacke, C.M. (2019). Metabolic adaptability in

550 metastatic breast cancer by AKR1B10-dependent balancing of glycolysis and fatty
551 acid oxidation. Nat Commun *10*, 2698. 10.1038/s41467-019-10592-4.

552 23. Raulien, N., Friedrich, K., Strobel, S., Rubner, S., Baumann, S., von Bergen, M.,
553 Körner, A., Krueger, M., Rossol, M., and Wagner, U. (2017). Fatty Acid Oxidation
554 Compensates for Lipopolysaccharide-Induced Warburg Effect in Glucose-Deprived
555 Monocytes. Front. Immunol. *8*, 609. 10.3389/fimmu.2017.00609.

556 24. Carta, G., Murru, E., Banni, S., and Manca, C. (2017). Palmitic Acid: Physiological
557 Role, Metabolism and Nutritional Implications. Front. Physiol. *8*, 902.
558 10.3389/fphys.2017.00902.

559 25. Koves, T.R., Li, P., An, J., Akimoto, T., Slentz, D., Ilkayeva, O., Dohm, G.L., Yan, Z.,
560 Newgard, C.B., and Muoio, D.M. (2005). Peroxisome Proliferator-activated Receptor-
561 γ Co-activator 1α-mediated Metabolic Remodeling of Skeletal Myocytes Mimics
562 Exercise Training and Reverses Lipid-induced Mitochondrial Inefficiency. J. Biol.
563 Chem. *280*, 33588-33598. 10.1074/jbc.m507621200.

564 26. Koves, T.R., Ussher, J.R., Noland, R.C., Slentz, D., Mosedale, M., Ilkayeva, O., Bain,
565 J., Stevens, R., Dyck, J.R.B., Newgard, C.B., et al. (2008). Mitochondrial Overload
566 and Incomplete Fatty Acid Oxidation Contribute to Skeletal Muscle Insulin
567 Resistance. Cell Metab. *7*, 45-56. 10.1016/j.cmet.2007.10.013.

568 27. Fendt, S.M., Frezza, C., and Erez, A. (2020). Targeting Metabolic Plasticity and
569 Flexibility Dynamics for Cancer Therapy. Cancer Discov. *10*, 1797-1807.
570 10.1158/2159-8290.Cd-20-0844.

571 28. Shim, J.-K., Choi, S., Yoon, S.-J., Choi, R.J., Park, J., Lee, E.H., Cho, H.J., Lee, S.,
572 Teo, W.-Y., Moon, J.H., et al. (2022). Etomoxir, a carnitine palmitoyltransferase 1
573 inhibitor, combined with temozolomide reduces stemness and invasiveness in patient-
574 derived glioblastoma tumorspheres. Cancer Cell Int. *22*, 309. 10.1186/s12935-022-
575 02731-7.

576 29. Adams, S.H., Hoppel, C.L., Lok, K.H., Zhao, L., Wong, S.W., Minkler, P.E., Hwang,
577 D.H., Newman, J.W., and Garvey, W.T. (2009). Plasma Acylcarnitine Profiles Suggest
578 Incomplete Long-Chain Fatty Acid β-Oxidation and Altered Tricarboxylic Acid Cycle
579 Activity in Type 2 Diabetic African-American Women. The Journal of Nutrition *139*,
580 1073-1081. https://doi.org/10.3945/jn.108.103754.

581 30. Koundouros, N., and Poulogiannis, G. (2020). Reprogramming of fatty acid
582 metabolism in cancer. Br. J. Cancer *122*, 4-22. 10.1038/s41416-019-0650-z.

583 31. Hui, S., Cowan, A.J., Zeng, X., Yang, L., Teslaa, T., Li, X., Bartman, C., Zhang, Z.,
584 Jang, C., Wang, L., et al. (2020). Quantitative Fluxomics of Circulating Metabolites.
585 Cell Metab. *32*, 676-688.e674. 10.1016/j.cmet.2020.07.013.

586 32. Neinast, M., Murashige, D., and Arany, Z. (2019). Branched Chain Amino Acids.
587 Annu. Rev. Physiol. *81*, 139-164. 10.1146/annurev-physiol-020518-114455.

588 33. Nyquist, M.D., Li, Y., Hwang, T.H., Manlove, L.S., Vessella, R.L., Silverstein,
589 K.A.T., Voytas, D.F., and Dehm, S.M. (2013). TALEN-engineered AR gene

590 rearrangements reveal endocrine uncoupling of androgen receptor in prostate cancer.
591 Proc. Natl. Acad. Sci. U. S. A. *110*, 17492-17497. doi:10.1073/pnas.1308587110.

592 34. Li, Y., Chan, S.C., Brand, L.J., Hwang, T.H., Silverstein, K.A., and Dehm, S.M.
593 (2013). Androgen receptor splice variants mediate enzalutamide resistance in
594 castration-resistant prostate cancer cell lines. Cancer Res. *73*, 483-489. 10.1158/0008-
595 5472.Can-12-3630.

596 35. Bishop, J.L., Thaper, D., Vahid, S., Davies, A., Ketola, K., Kuruma, H., Jama, R., Nip,
597 K.M., Angeles, A., Johnson, F., et al. (2017). The Master Neural Transcription Factor
598 BRN2 Is an Androgen Receptor–Suppressed Driver of Neuroendocrine
599 Differentiation in Prostate Cancer. Cancer Discov. *7*, 54-71. 10.1158/2159-8290.Cd-
600 15-1263.

601 36. Nagarajan, S.R., Paul-Heng, M., Krycer, J.R., Fazakerley, D.J., Sharland, A.F., and
602 Hoy, A.J. (2019). Lipid and glucose metabolism in hepatocyte cell lines and primary
603 mouse hepatocytes: a comprehensive resource for in vitro studies of hepatic
604 metabolism. Am J Physiol Endocrinol Metab *316*, E578-E589.
605 10.1152/ajpendo.00365.2018.

606 37. Parmenter, T.J., Kleinschmidt, M., Kinross, K.M., Bond, S.T., Li, J., Kaadige, M.R.,
607 Rao, A., Sheppard, K.E., Hugo, W., Pupo, G.M., et al. (2014). Response of BRAF-
608 mutant melanoma to BRAF inhibition is mediated by a network of transcriptional
609 regulators of glycolysis. Cancer Discov. *4*, 423-433. 10.1158/2159-8290.CD-13-0440.

610 38. Chambers, M.C., Maclean, B., Burke, R., Amodei, D., Ruderman, D.L., Neumann, S.,
611 Gatto, L., Fischer, B., Pratt, B., Egertson, J., et al. (2012). A cross-platform toolkit for
612 mass spectrometry and proteomics. Nat. Biotechnol. *30*, 918-920. 10.1038/nbt.2377.
613